Ultrafast disordering of vanadium dimers in photoexcited VO_2

Simon Wall[1,*,†], Shan Yang[2,†] Luciana Vidas[1], Matthieu Chollet[3], Michael Glownia[3], Michael Kozina[4], Tetsuo Katayama[5], Thomas Henighan[4], Mason Jiang[4], Timothy A. Miller[1], David A. Reis[4,6,7], Lynn A. Boatner[8], Olivier Delaire[2,9,*], Mariano Trigo[4,6,*]

Affiliations:

1 ICFO - Institut de Ciències Fotòniques, The Barcelona Institute of Science and Technology, 08860 Castelldefels (Barcelona), Spain

2 Department of Mechanical Engineering and Materials Science, Duke University, Durham, NC 27708, USA.

3 Linac Coherent Light Source, SLAC National Accelerator Laboratory, Menlo Park, California 94025, USA.

4 Stanford PULSE Institute, SLAC National Accelerator Laboratory, Menlo Park, CA

5 Japan Synchrotron Radiation Research Institute, 1-1-1 Kouto, Sayo-cho, Sayo-gun, Hyogo 679-5198, Japan

6 Stanford Institute for Materials and Energy Science, SLAC National Accelerator Laboratory, Menlo Park, CA.

7 Department of Applied Physics, Stanford University

8 Materials Science and Technology Division, Oak Ridge National Laboratory, Oak Ridge, TN 37831, USA,

9 Department of Physics, Duke University, Durham, NC 27708, USA

*Correspondence to: simon.wall@icfo.eu olivier.delaire@duke.edu mtrigo@slac.stanford.edu

† These authors provided equal contribution

Abstract:

Many ultrafast solid phase transitions are treated as chemical reactions that transform the structures between two different unit cells along a reaction coordinate, but this neglects the role of disorder. While ultrafast diffraction provides insights into atomic dynamics during such transformations, diffraction alone probes an averaged unit cell and is less sensitive to randomness in the transition pathway. Using total scattering of femtosecond x-ray pulses, we show that atomic disordering in photoexcited VO_2 is central to the transition mechanism and that, after photoexcitation, the system explores a large volume of phase-space in a timescale comparable with a single phonon oscillation. These results overturn the current understanding of an archetypal ultrafast phase transition and provide new microscopic insights into rapid evolution toward equilibrium in photoexcited matter.

One Sentence Summary: Total X-ray scattering on VO_2 reveals that rapid, random disorder and an increase in lattice entropy achieves ergodicity on the ultrafast timescale and drives the insulator-metal phase transition.

Main Text:

Manipulating the structure and function of materials remains one of the ultimate challenges of modern science and technology *(1)*. Ultrafast pulses can create novel phases not accessible in equilibrium by transiently modifying the interatomic potential *(2-4)* and the atomic positions *(5-7)*. However, probing the short-lived transient structures of 10^{23} atoms is a challenge, and the dynamics are often simplified by assuming they evolve on a potential energy surface described by a few degrees of freedom with a well-defined spatial periodicity (*3,8-11*). Although ultrafast electron *(8,12,13)* and x-ray diffraction *(2, 10, 14-17)* are sensitive to the structure with atomic length-scale and femtosecond time resolution, they measure averages over many unit cells, and thus are less sensitive to random displacements. To overcome this limitation, we use femtosecond total x-ray scattering *(18)* to study the dynamics of the structural transition of bulk VO_2 at all length-scales. We observe that the structural transition proceeds by uncorrelated disordering of the vanadium ions from their initial dimerized distribution, rather than the previously proposed synchronized motion along an optical phonon mode *(8, 12, 14, 19)*. Supported by ab-initio molecular dynamics, our results show that the highly anharmonic, flat potential energy surface allows the quasi-rutile structure in the photoexcited state to develop on femtosecond timescales, by disrupting the vanadium pairs and populating a continuum of modes that enables the system to reach ergodicity within 150 fs. More generally, these results question the common interpretation of many ultrafast measurements in terms of motion along a well-defined reaction coordinate, or order parameter, on a potential energy surface (*5, 8, 10, 12, 16, 20)* and provide a new level of understanding regarding how complex systems can reach ergodicity on an ultrafast timescale.

Ultrafast structural transitions are usually described in terms of a few phonon modes with well-defined wavevectors and it is assumed that the system evolves along a potential surface connecting the initial and final structures which also determines the speed of the photoexcited transition *(2-4,14,19)*. However, this assumes a coordinated motion along a well-defined reaction coordinate and ignores the role of disorder and entropy, which are thought to develop on slower timescales, even though entropy may be the driving factor in the thermodynamic transition *(21)*. To date, all attempts to measure the "molecular movie" of the dynamics of a phase transition at the atomic scale have exploited Bragg scattering, which can only measure the average motions of atoms and is insensitive to deviations from the average reaction coordinate. Using femtosecond pulses from a Free Electron Laser (FEL), we measured total x-ray scattering, containing discrete Bragg peaks as well as the diffuse continuum between them, and show that the lattice disorder in photoexcited VO_2, manifested as diffuse intensity across momentum-space, reaches close to its equilibrium value in a timescale comparable to a single atomic oscillation.

Vanadium dioxide (VO_2) can be switched from an insulating to a metallic state with ultrafast pulses. The insulator-to-metal transition (IMT) is accompanied by a structural change from a monoclinic (M1) to a rutile (R) structure (Fig. 1a,b), and numerous prior efforts have focused on elucidating the evolution of both the electronic and lattice degrees of freedom via ultrafast pump-probe measurements *(4, 8, 9, 12, 14, 21*). Generally, a solid-solid phase transition where the symmetry of the crystal is raised (from M1 to R in VO_2) as the temperature increases can be dominated by either a displacive process or an order-disorder process (Fig. 1c,d). The distortion at the IMT in VO_2 has widely been interpreted as a displacive transition corresponding to a phonon soft-mode of the high-symmetry metallic phase, based on symmetry considerations, diffraction measurements, as well as lattice dynamics simulations *(8, 12, 22-25*). In a displacive

transition, the atoms collaboratively reshuffle their positions under the effect of one or few well-defined, spatially-coherent vibrational modes, of amplitude ξ, that link the low- and high-symmetry structures. This is illustrated for the dimerized vanadium pairs of the monoclinic (M1) phase of VO_2 in Fig. 1c, with wave-vector at the R point in the rutile Brillouin zone, $\mathbf{k}^{(R)} = (0,½,½)_R$ (here subscripts denote the Bravais basis convention (M1 or R), while the superscript (R) represents the special point in the Brillouin zone). Below the critical temperature, T_c = 340 K, the system is locked near an energy minimum at a large amplitude of ξ, yielding the structural distortion and additional superstructure diffraction peaks, owing to the doubling of the unit cell volume, represented by the red dots in Fig. 1e. Above T_c, the onset of a displacive mechanism would show characteristic soft phonons at the associated wave-vector (red crosses at $\mathbf{k}^{(R)}$ in Fig. 1f, corresponding to additional Brillouin zone centers in Fig. 1e) *(26-28)*. Alternatively, in an order-disorder transition, the atoms move from the low- to the high-symmetry structure in a spatially incoherent manner with no characteristic correlation length *(26, 28)* and without soft modes at any wave-vector (Fig. 1d). The two possible types of transformation can be distinguished by probing for diffuse intensity extended across reciprocal space, which is a hallmark of large amplitude motions due to the uncorrelated disorder (orange shaded areas, Fig. 1g). Importantly, in both cases the average atomic position may follow the same trajectory, and thus an ultrafast diffraction measurement probing the Bragg peaks alone cannot distinguish between displacive and order-disorder mechanisms (Fig. 1h,i).

Optical probes of photo-excited VO_2 show that coherent optical lattice vibrations are induced for low intensity excitation *(4,9,19)*. At the same time, structural probes *(8, 12)* have shown that the long-range order of the V dimerization is lost in < 300 fs, but these measurements lacked the sub-100 fs time resolution required to probe the transition on the timescale of relevant vibrational periods. Furthermore, these experiments lacked sensitivity to deviations from average lattice periodicity at arbitrary wavevectors, which are a signature of disorder in the transition mechanism. Here, we use femtosecond total x-ray scattering (~50 fs time resolution) with an x-ray free electron laser (FEL) to obtain a more complete picture of the dynamics during the photo-induced structural transition in VO_2. We observe a rapid disordering of the low temperature structure that starts as soon as 50 fs after photoexcitation, as observed through a rapid increase in diffuse x-ray intensity and an equally fast decrease in the intensity of the Bragg peaks of the low symmetry structure. Furthermore, the diffuse intensity distribution in reciprocal space at 150 fs resembles the rutile equilibrium distribution, and suggests that the lattice reaches a near ergodic state in that timescale. This unequivocally shows that the non-equilibrium photoinduced transition is of the order-disorder type, driven by an ultrafast change in the lattice potential that suddenly unlocks the vanadium dimers and yields large-amplitude uncorrelated motions, rather than occurring along a coherent displacive coordinate. Our ab-initio molecular dynamics (AIMD) simulations based on density functional theory (DFT) potentials corroborate the observed ultrafast timescale of the disordering. The DFT calculations show that the ionic potential in the photoexcited phase is highly anharmonic and flat, which explains the observed large vanadium displacements, and is also the origin of the high phonon entropy of the equilibrium metallic phase *(21)*.

Total X-ray scattering patterns were collected with 9.5 keV photons at the XPP end station at LCLS from high quality single crystals of VO_2, see methods for details (*29*). The difference in the equilibrium scattering for T = 353 K (R) and T = 295 K (M1) is shown in Fig. 2a (see Fig. S2 for M1 and R raw patterns (*29*)). The change is dominated by the suppression of three strong Bragg peaks of the M1 phase labelled $(-1\ 0\ -2)_{M1}$, $(-1\ 2\ 0)_{M1}$ and $(-1\ 2\ 2)_{M1}$. In

addition, a rectangular-shaped diffuse feature strongly increases in intensity. Our simulations of the change in the total scattering (Figs. 2b), based on the equilibrium force constants obtained from density functional theory (DFT, see Methods (*29*)) reproduce the diffuse signature well, and indicate that it originates from soft transverse acoustic phonons of the rutile phase *(21)*. This enables the vanadium atoms to adopt a large distribution of displacements about their average positions in the rutile phase.

In Fig. 2c we show the photo-induced changes in the total scattering 350 fs after photoexcitation for an absorbed pump fluence of 20 mJ/cm^2, in the saturation regime for the photoinduced phase transition (*19*). The photo-induced changes in the total scattering show a striking resemblance to the thermal changes in Fig 2a. The intensities of the Bragg peaks are strongly suppressed due to the change in the crystalline symmetry, while the extended diffuse scattering strongly increases. This shows that on this very fast timescale, not only has the long-range, average symmetry of the crystal changed, as indicated by the fast suppression of the M1 peaks, but also the vanadium atoms have already adopted a rutile-like displacement distribution.

Before turning to the timescale in more detail, we examine the fluence dependence of the photo-induced phase transition. Figure 2d shows the fluence dependence of the $(-1\ 2\ 0)_{M1}$ Bragg peak and the integrated diffuse scattering at approximately 350 fs and 500 ps after excitation. The Bragg peak shows a linear decrease in intensity with absorbed fluence for fluences below a threshold of $F_c \sim 5$ mJ/cm^2, after which the change is more rapid until saturation and complete suppression occurs. The Bragg peak dynamics also change significantly below and above threshold, with coherent phonons observed to modulate the Bragg intensity below threshold, while the coherent signal disappears above threshold (Fig S11), in agreement with optical measurements (*4*). The diffuse scattering also shows threshold-like behavior, rising abruptly above $F_c \sim 5$ mJ/cm^2, indicating that the vanadium ions only adopt the broad, rutile-like distribution above a critical fluence.

We now turn to the dynamics of this process. Figure 3a shows the change in intensity $\Delta I(\mathbf{Q}, t)$ at delays of 50 fs, 100 fs, and 2 ps for excitation in the saturation regime. It is clear that changes in the diffuse scattering already begin to occur over extended portions of reciprocal space within 50 fs of photoexcitation and the **Q** dependence of the scattering shows little subsequent change after reaching its full intensity at about 150 fs. To examine this timescale in more detail we follow the temporal evolution of the intensity for specific regions of reciprocal space. Figure 3b shows the dynamics of multiple Bragg peaks and of the diffuse scattering intensity in the high-fluence regime. All curves clearly show that the timescale for the structural transition is at least twice faster than the 300 fs reported from previous diffraction measurements *(8, 12)*. Importantly, this timescale is above the ~ 50 fs experimental time resolution. The timescale for the rise of the integrated diffuse intensity is independent of fluence above the threshold, as shown in Fig S12. Below threshold and at long delays, the Bragg peaks can be affected by strain, which leads to slow changes in intensity at the few ps timescale.

The dynamics of both the Bragg peaks and diffuse scattering observed here indicate a direct structural transition between the M1 and R phase, without evidence of passing through intermediate structures previously reported *(12)*. M1 superstructure peaks (e.g. $(-1\ 0\ -2)_{M1}$, $(-1\ 2\ 0)_{M1}$) are not present in the rutile structure and all rapidly drop to zero intensity. Peaks labeled R are present in both phases and can initially increase or decrease depending on their structure factor response to the average distortion, $F_{hkl}(\xi)$. Importantly, the diffuse scattering signal changes on the same timescale as the Bragg peaks, showing that the disordering occurs as fast as

the loss of M1 long-range order. This indicates that the phase transition is dominated by disordering of the vanadium ions rather than a coherent atomic motion along the ξ coordinate.

In order to gain greater insight into the phase-change dynamics, we performed ab initio molecular dynamics (AIMD) simulations of the photo-induced phase transition. The lattice potential was obtained from DFT, including electronic correlation effects at the level of PBE+U, and the effect of photoexcitation was modelled as a sudden increase in the electronic temperature, T_{el}, see supplementary information for details (*29*). The relaxed ground-state structure in the M1 phase shows a clear threshold behavior in T_{el} above which the V dimerization disappears (Fig. S4), leading to a rutile-like phase, similar to the trend observed with increasing hole concentration (*30*), and in agreement with the experimental observation of a threshold laser fluence. The time-dependent Bragg intensities derived from the ionic positions after electronic excitation are plotted in Fig. 3b together with the measured diffraction signals. An excellent agreement is obtained both in terms of the timescale for the dynamics and the amplitude of the change. The agreement is truly remarkable considering that the only adjustable parameter was the global temporal offset between the data and the simulation.

Figure 4a shows the AIMD evolution of short dimerized bonds (d_S) and long V-V bonds (d_L) along the rutile *c*-axis, after a sudden increase in T_{el} at $t = 0$, starting with a thermal M1 structure at 300 K. Bond-length distributions, averaged over specified time windows, are shown in Fig. 4b. The initial distribution is bimodal (d_S = 2.50 Å, d_L = 3.16 Å), reflecting the monoclinic dimerization pattern (Fig. 1a). After the prompt transition, it quickly collapses to the unimodal distribution expected for the rutile phase, $d_S = d_L$ = 2.81 Å = d_R. Already within the first 75 femtoseconds, the tails of the distributions show some vanadium pairs with the rutile bond length, but the means only cross at about 150 fs, and slightly overshoot the ideal rutile bond length at $t \sim 200$ fs before rebounding, resulting in a damped oscillation converging to the equidistant configuration. This overshoot is responsible for the single-cycle overdamped oscillation in the $(-1\ 0\ -2)_{M1}$ and $(-1\ -1\ 3)_{M1}$ peaks. Similar dynamics are observed in the evolution of the twist angle, and the frequency of the damped oscillation is about 3 THz (Fig. S5), but is doubled (~6 THz) in the diffraction data shown in Fig. 3b because $|F_{hkl}(\xi)|^2 \sim \xi^2$ when $d_L = d_S = d_R$.

Our measurements, confirmed by simulations, show that the changes in bond length and angle occur concomitantly and within a few hundred femtoseconds, in contrast to previous scenarios based on analysis of time resolved electron Bragg scattering alone (8). The vibrational modes at 3 THz are significantly slower than the 6 THz mode previously suggested to limit the phase transition *(19)*, but agrees well with the frequency of V-dominated flat transverse acoustic modes of the R phase, as seen in our first-principles simulations of the phonon density-of-states (Fig. 4d) and dispersions (Supplement Fig. 6d), showing that no single wave-vector is responsible for the transition. In addition, the dynamics of the standard deviation is consistent with the timescale of the diffuse scattering (solid line and symbols in Fig. 3b, top trace), further demonstrating that a broad distribution of modes is required to describe the evolution of the distribution of displacements in Figs. 4a-b. The AIMD simulations thus indicate that photo-excitation drives an instantaneous change in the lattice potential leading to rutile-like dynamics of the vanadium ions. The effect of changing the electronic temperature on the potential energy surface along the distortion ξ (M1-to-R distortion in Fig. 1c) is shown in Fig. 4c. As can be seen, the electronic excitation results in the loss of the double-well potential characteristic of the M1

phase and instead stabilizes the flat, strongly anharmonic quartic-like potential of the rutile phase.

These observations allow us to build a radically new description of the photo-induced phase transition in VO_2. To date, most theoretical models and interpretations of experimental data have assumed a transition driven coherently by phonon modes of well-defined wavevector (typically $\mathbf{k}_R$) and frequency (*8, 9, 12, 14, 19*), and have ignored the role of fluctuations and disorder. Our combined ultrafast total scattering measurements and first-principles simulations of dynamics show that ultrafast disordering is a key aspect of the photoexcited state of VO_2. Photoexcitation instantaneously creates a new lattice potential, which can be described by a hot electron distribution within the DFT framework. The new potential quickly alters the dynamics of vanadium ions, effectively severing the intra-dimer spring constant, causing them to rapidly assume the new high-symmetry configuration. We note that these V-V interactions in the rutile phase yield a flat, dispersive-less transverse acoustic phonon branch (*21*). These features of the potential cause the transformation to proceed without spatial coherence and no well-defined wavevector.

The timescale of this disordering process is another particularly surprising observation. The rapid excitation of phonons in a broad range of wave vectors, observed through the diffuse scattering and occurring within 150 fs, is significantly faster than other disorder-driven phase transitions *(13, 17)*. We note that, while the speed of a soft-mode-driven transition is governed by the curvature of the potential surface along the ξ coordinate *(3)*, the non-equilibrium order-disorder transition timescale reflects the time for the displacements to become uncorrelated and reach a quasi-equilibrium distribution. The dynamics observed here are fast because the average distance between M1 and rutile is relatively short (ξ_0 = 0.24 Å, the position of the minimum of the potential in Fig. 4c). Indeed, the average vanadium velocity at room temperature is 3.8 Å/ps so they could traverse the distance ξ_0 in ~ 60 fs. While this is a simplified model, the flatness of the photoexcited potential in Fig.4c suggests that the dynamics are partially inertial and that the speed of the transition is mainly limited by the initial thermal distribution of velocities in the M1 phase, and the amplitude of the M1-to-R distortion. The change in the potential produces an ultrafast activation of a large number of low-energy V-dominated phonon modes spread out in reciprocal space, as seen in the broadly distributed diffuse scattering signal, and in the phonon dispersions in Fig S6. The rapid evolution toward ergodicity is thus enabled by the large phase space with low-frequency V-dominated transverse acoustic modes, which was also noted in *(21)* to yield a large phonon entropy gain stabilizing the rutile phase, and the strong damping of phonons in the rutile phase. Our current observations thus reveal an interesting parallel to the thermal transition.

Our results show that the structural transformation in VO_2 occurs along many concurrent degrees of freedom spanning a large phase-space, and thus a complete description must extend beyond that of a single order parameter or discrete set of displacements. The rapid, large-amplitude disordering observed here is caused by the flatness of the photoexcited potential and is intimately related with the high entropy of the rutile phase *(21)*; but the implications of our findings, in fact, extend well beyond the VO_2 system. The role of disorder has been neglected in many ultrafast solid-solid phase transitions, even though the ultimate control of properties on demand relies on a reversible pathway between the two states. Our findings suggest that disorder may play an important role in some materials and that a description in terms of a single degree of freedom is incomplete. This disorder presents both opportunities as well as challenges to ultrafast material

control. Disorder ultimately prevents coherent control of phase transitions, and complete control over the phase transition pathway. However, transient disorder can become a new knob by which materials can be controlled, just as disordered solids (glasses) can show dramatic differences to their crystalline counterparts in near-equilibrium conditions. Understanding whether disorder plays a general role in vibrationally excited solids *(7)* could ultimately provide a new perspective on how to control matter, specifically could suggest a new direction in which light-induced superconductivity may be achieved *(5)*.

References and Notes:

1. Basov, D. N., Averitt, R. D. & Hsieh, D. Towards properties on demand in quantum materials. *Nat. Mater.* **16,** 1077–1088 (2017).
2. Fritz, D. M. *et al.* Ultrafast Bond Softening in Bismuth: Mapping a Solid's Interatomic Potential with X-rays. *Science* **315,** 633–636 (2007).
3. Huber, T. *et al.* Coherent structural dynamics of a prototypical charge-density-wave-to-metal transition, *Phys. Rev. Lett.* **113,** 026401 (2014).
4. Wall, S. *et al.* Ultrafast changes in lattice symmetry probed by coherent phonons. *Nat. Commun.* **3,** 721 (2012).
5. Mankowsky, R. *et al.* Nonlinear lattice dynamics as a basis for enhanced superconductivity in $YBa_2Cu_3O_{6.5}$. *Nature* **516,** 71–73 (2014).
6. Katayama, I. *et al.* Ferroelectric Soft Mode in a $SrTiO_3$ Thin Film Impulsively Driven to the Anharmonic Regime Using Intense Picosecond Terahertz Pulses. *Phys. Rev. Lett.* **108,** 97401 (2012).
7. Först, M. *et al*. Nonlinear phononics as an ultrafast route to lattice control. *Nat. Phys.* **7**, 854-856 (2011)
8. P. Baum, D.-S. Yang, and A. H. Zewail, 4D Visualization of Transitional Structures in Phase Transformations by Electron Diffraction, *Science* **318**, 788–792 (2007).
9. Kübler, C. *et al.* Coherent structural dynamics and electronic correlations during an ultrafast insulator-to-metal phase transition in VO_2. *Phys. Rev. Lett.* **99,** 116401 (2007).
10. Beaud, P. *et al.* A time-dependent order parameter for ultrafast photoinduced phase transitions. *Nat. Mater.* **13,** 923–927 (2014).
11. Hellmann, S. *et al.* Time-domain classification of charge-density-wave insulators. *Nat. Commun.* **3**, 1069 (2012).
12. Morrison, R. *et al.* . A photoinduced metal-like phase of monoclinic VO_2 revealed by ultrafast electron diffraction, *Science* **346,** 445 (2014).
13. Waldecker, L. *et al.* Time-domain separation of optical properties from structural transitions in resonantly bonded materials. *Nat. Mater.* **14,** 991–995 (2015).
14. Cavalleri, A. *et al.* Femtosecond Structural Dynamics in VO_2 during an Ultrafast Solid-Solid Phase Transition. *Phys. Rev. Lett.* **87,** 237401 (2001).

15. Hada, M., Okimura, K. & Matsuo, J. Characterization of structural dynamics of VO_2 thin film on *c*-Al_2O_3 using in-air time-resolved X-ray diffraction. *Phys. Rev. B* **82**, 153401 (2010).

16. Ichikawa, H. *et al.* Transient photoinduced 'hidden' phase in a manganite. *Nat. Mater.* **10,** 101–105 (2011).

17. Lindenberg, A. M. *et al.* Atomic-Scale Visualization of Inertial Dynamics. *Science.* **308,** 392–395 (2005).

18. Trigo, M. *et al.* Fourier-transform inelastic X-ray scattering from time- and momentum-dependent phonon-phonon correlations. *Nat Phys* **9,** 790–794 (2013).

19. Cavalleri, A., Dekorsy, T., Chong, H. H. W., Kieffer, J. C. & Schoenlein, R. W. Evidence for a structurally-driven insulator-to-metal transition in VO_2: A view from the ultrafast timescale. *Phys. Rev. B* **70,** 161102(R) (2004).

20. Kolobov, A. V., Krbal, M., Fons, P., Tominaga, J. & Uruga, T. Distortion-triggered loss of long-range order in solids with bonding energy hierarchy. *Nat. Chem.* **3,** 311–316 (2011).

21. Budai, J. D. et al, "Metallization of vanadium dioxide driven by large phonon entropy", Nature **515**, 535–539 (2014).

22. Brews, J. R., Symmetry Considerations and the Vanadium Dioxide Phase Transition, *Phys. Rev. B* **1**, 2557 (1970).

23. Gupta, M. Freeman, A. J., Ellis, D. E., "Electronic structure and lattice instability of metallic VO_2, *Phys. Rev. B* **16**, 3338 (1977).

24. Terauchi, H. and Cohen, J. B. , Diffuse x-ray scattering due to the lattice instability near the metal-semiconductor transition in VO_2, *Phys. Rev. B* **17**, 2494 (1978).

25. Gervais, F., Kress, W., "Lattice dynamics of oxides with rutile structure and instabilities at the metal-semiconductor phase transitions of NbO_2 and VO_2", *Phys. Rev. B* **31**, 4809 (1985).

26. Bruce, A. D. Structural phase transitions. II. Static critical behaviour. *Adv. Phys.* **29,** 111–217 (1980).

27. Cowley, R. A. Structural phase transitions I. Landau theory. *Adv. Phys.* **29,** 1–110 (1980).

28. Dove, M. T. Theory of displacive phase transitions in minerals. *Am. Mineral.* **82,** 213–244 (1997).

29. Materials and methods are available as supplementary materials

30. Yuan, X., Zhang, W. & Zhang, P. Hole-lattice coupling and photoinduced insulator-metal transition in VO_2. *Phys. Rev. B* **88,** 035119 (2013).

31. Chollet, M., et al, *J. Synchrotron Rad.* **22**, 503 (2015)

32. Verleur, H. W., Barker, Jr, A. S. and Berglund, C. N. , Optical properties of VO_2 between 0.25 and 5 eV. *Phys. Rev.* **172**, 788 (1968)

33. Kresse, Georg, and Jürgen Hafner. "Ab initio molecular dynamics for liquid metals." *Phys. Rev. B* **47**, 558 (1993).

34. Kresse, Georg, and Jürgen Furthmüller. "Efficient iterative schemes for ab initio total-energy calculations using a plane-wave basis set." *Phys. Rev. B* **54**, 11169 (1996).

35. Blochl, P. E. Projector augmented-wave method. *Phys. Rev. B* **50**, 17953 (1994)

36. Kresse, G. and Joubert, D. From ultrasoft pseudopotentials to the projector augmented-wave method. *Phys. Rev. B* **59**, 1758–1775 (1999)

37. Perdew, J.P., Burke, K, and Ernzerhof, M. Generalized gradient approximation made simple. *Phys. Rev. Lett*. **77**, 3865–3868 (1996)

38. Liebsch, A., H. Ishida, and G. Bihlmayer. Coulomb correlations and orbital polarization in the metal-insulator transition of VO_2. *Phys. Rev. B* **71**, 085109 (2005)
39. Longo, J. M. & Kierkegaard, P. A refinement of the structure of VO_2. *Acta Chem. Scand.* **24**, 420–426 (1970)
40. McWhan, D. B., Marezio, M., Remeika, J. P. & Dernier, P. D. X-ray-diffraction study of metallic VO_2. *Phys. Rev. B* **10**, 490–495 (1974)
41. Togo, Atsushi, and Isao Tanaka. First principles phonon calculations in materials science. *Scr. Mater*. **108**, 1-5 (2015)
42. Hellman, Olle, Peter Steneteg, Igor A. Abrikosov, and Sergei I. Simak. Temperature dependent effective potential method for accurate free energy calculations of solids. *Physical Review B* **87**, 104111 (2013)
43. Lee, Sangwook, Kedar Hippalgaonkar, Fan Yang, Jiawang Hong, Changhyun Ko, Joonki Suh, Kai Liu et al. "Anomalously low electronic thermal conductivity in metallic vanadium dioxide." *Science* **355**, 371-374, (2017)
44. Waseda, Yoshio, Matsubara, Eiichiro, Shinoda, Kozo. X-ray diffraction crystallography: introduction, examples and solved problems. *Springer Science & Business Media* (2011).
45. Róg, Tomasz, Krzysztof Murzyn, Konrad Hinsen, and Gerald R. Kneller. nMoldyn: a program package for a neutron scattering oriented analysis of molecular dynamics simulations. *J. Comput. Chem.* **24**, 657-667 (2003)
46. Marezio, M., Do B. McWhan, J. P. Remeika, and P. D. Dernier. Structural Aspects of the Metal-Insulator Transitions in Cr-Doped VO_2. *Phys. Rev. B* **5**, 2541 (1972).
47. Eyert, Volker. The metal-insulator transitions of VO_2: A band theoretical approach. *Ann. Phys. (Leipzig)* 11 650-704 (2002)
48. Aroyo, M. I. , Orobengoa, D. , de la Flor, G., Tasci, E.S., Perez-Mato J. M., and Wondratschek, H. "Brillouin-zone databases on the Bilbao Crystallographic Server". Acta. Cryst. A70 126-137 (2014)

Acknowledgments:
Preliminary static diffuse scattering patterns were collected at the 11-3 beamline of the Stanford Synchrotron Radiation Light Source (SSRL).

Funding: Work at ICFO was supported by Spanish MINECO (Severo Ochoa grant SEV-2015-0522), Ramón y Cajal programme RYC-2013-14838 and Fondo Europeo de Desarrollo Regional FIS2015-67898-P (MINECO/FEDER) as well as Marie Curie Career Integration Grant PCIG12-GA-2013-618487, Fundació Privada Cellex, and CERCA Programme / Generalitat de Catalunya. First-principles simulations and analysis (SY, OD) were supported by the U.S. Department of Energy, Office of Science, Basic Energy Sciences, Materials Sciences and Engineering Division, under the Early Career Award No. DE-SC0016166. MK, TH, MT and DAR were supported by

the U.S. Department of Energy, Office of Science, Office of Basic Energy Sciences through the Division of Materials Sciences and Engineering under Contract No. DE-AC02-76SF00515. Use of the Linac Coherent Light Source (LCLS), and the Stanford Synchrotron Radiation Lightsource at SLAC National Accelerator Laboratory, is supported by the U.S. Department of Energy, Office of Science, Office of Basic Energy Sciences under Contract No. DE-AC02-76SF00515. Additional X-ray measurements were performed at BL3 of SACLA with the approval of the Japan Synchrotron Radiation Research Institute (JASRI) (Proposal No. 2016A8008). Ab-initio calculations were performed using resources of the National Energy Research Scientific Computing Center, A U. S. DOE Office of Science User Facility supported by the Office of Science of the U. S. Department of Energy under Contract No. DE-AC02-05CH11231. First principles simulations for this research used resources of the Oak Ridge Leadership Computing Facility at the Oak Ridge National Laboratory, which is supported by the Office of Science of the U.S. Department of Energy under Contract No. DE-AC05-00OR22725.

Author contributions: L. V, M. C, M. G, M. K., T. K., T. H., M. J., T. A. M., D. A. R., O. D. contributed to the data collection led by S. W. and M. T. Data analysis was performed by S.W and M.T. Sample synthesis was performed by L.A.B. S.Y. performed DFT calculations under the supervision of O.D. S. W., O.D. and M. T. proposed, planned and coordinated all aspects of the project.

Competing interests: Authors declare no competing interests.

Data and materials availability: All data needed to evaluate the conclusions in the paper are present in the paper or the supplementary materials.

Supplementary Materials:

Materials and Methods

Figures S1-S12

Movies S1-S2

References (*31-48*)

Figures:

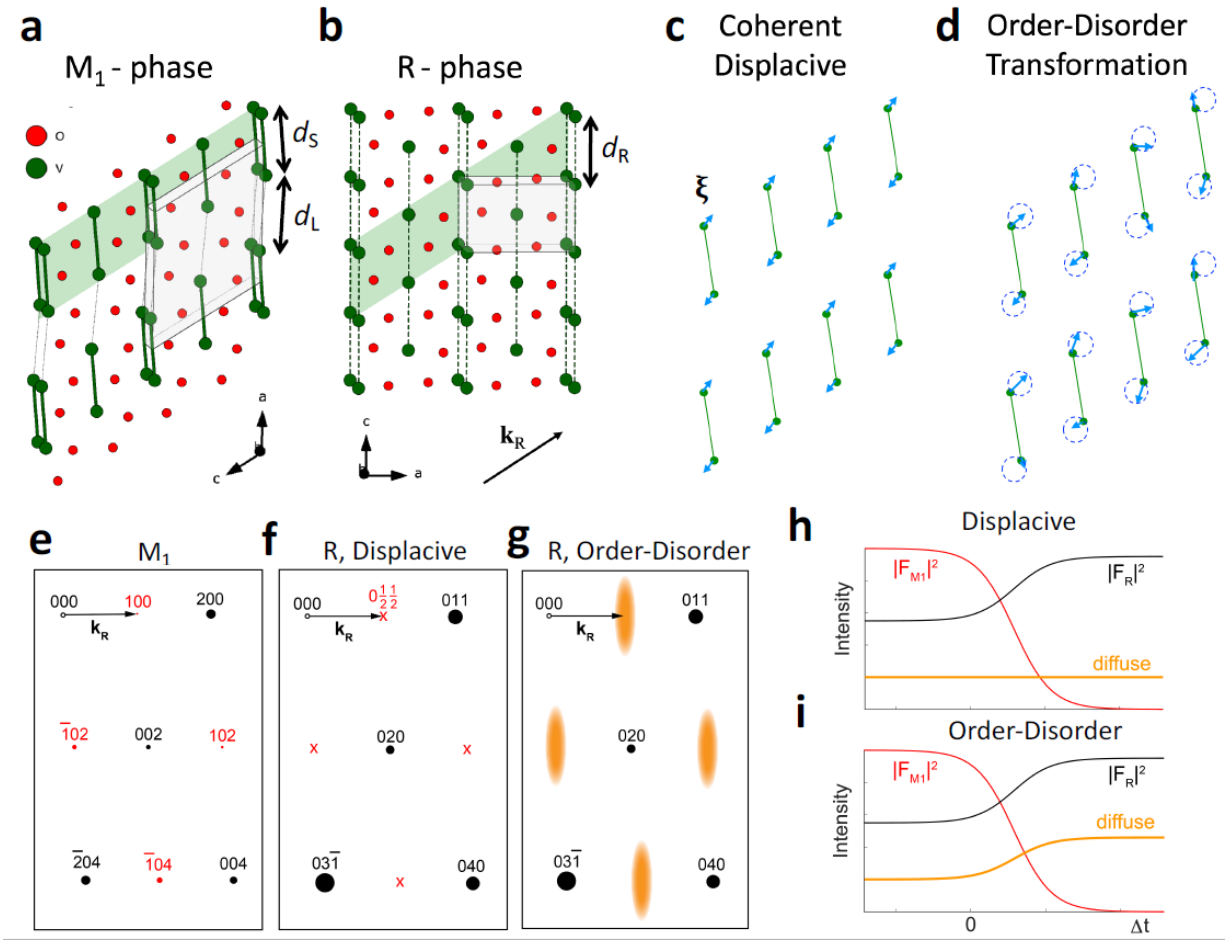

Fig. 1. VO_2 structural distortion in real and reciprocal space **(A,B)** Correspondence between the M_1 and R phases, highlighting the pattern of dimerization of V pairs along the rutile (R) c-axis, leading to diagonal layers of tilted dimers (green bands), along the wave-vector corresponding to the modulation of the R-phase, $\mathbf{k}^{(R)}$ = (½,0,½) or (0,½,½) r.l.u. Grey boxes represent the unit cell of each structure. **(C,D)** Alternate possible transition mechanisms between the M_1 phase and the R phase upon photoexcitation. The spatially-coherent distortion **(C)** with coordinate ξ is a symmetry-allowed transformation path between R and M1, which matches low-energy phonon excitations of the rutile phase at the R point, localized at $\mathbf{k}^{(R)}$ in reciprocal space. The disordering mechanism **(D)** has no well-defined wavevector and causes extended diffuse scattering in **k**-space. Diffractograms for the **(E)** M_1 phase and **(F,G)** rutile-like phases resulting from either displacive distortion **(F)** or a disordering transition **(G)**. Note the appearance in M_1 of superstructure Bragg peaks at $\mathbf{k}^{(R)}$ points of the rutile phase (crosses at coordinates with half integers in R phase). The shaded orange regions in **(G)** represent a diffuse scattering intensity that is more extended than the exact $\mathbf{k}^{(R)}$ modulation wavevector. **(H,I)** Schematic time evolutions of the intensity of Bragg peaks for M_1 and R phases and diffuse signal, for a

displacive transition **(H)** or an order-disorder transition **(I)**. Zero time corresponds to photoexcitation.

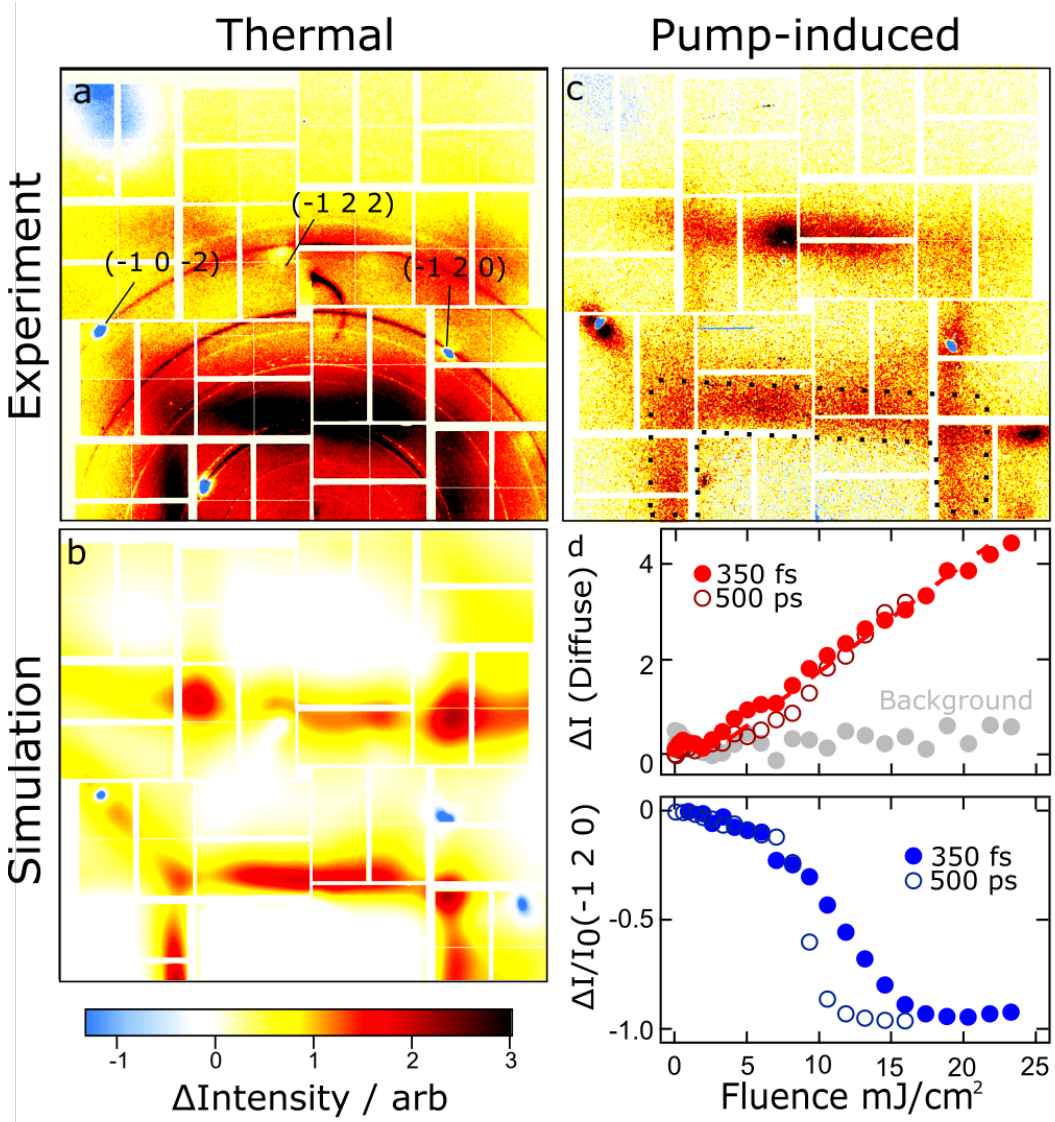

Fig. 2. Diffuse scattering from the thermal and photo induced phase transitions in VO_2 Saturated false-color plot of the difference in the thermal diffuse scattering intensity between the R (353 K) and the M1 phases at (295 K) (ΔI(**Q**) = I(**Q**,353 K) - I(**Q**, 295 K)), **(A)** measured at LCLS and **(B)** calculated based on the equilibrium force constants. The positions of several Bragg peaks are indicated. The rings in **(A)** arise from X-ray scattering at damaged edges of the sample and the central semicircle-like feature corresponds to laser scatter, see methods and Figs. S1 and S2 for details (*29*). **(C)** Pump-induced change in the scattering signal when excited at 20 mJ/cm^2 at fixed delay of 350 fs (ΔI(**Q**) = I(**Q**,350 fs) - I(**Q**, -11 ns)) showing very similar changes to the thermal response. **(D)** Pump fluence dependence of the $(-1,2,0)_{M1}$ peak amplitude and mean diffuse scattering as integrated over the boxed area in at 350 fs and 500 ps. The gray dots represent the background taken as the mean intensity at low scattering angles. **(C)**. A linear

fit (dashed line) to the high fluence part of the diffuse scattering gives a threshold of F_c~5 mJ/cm^2.

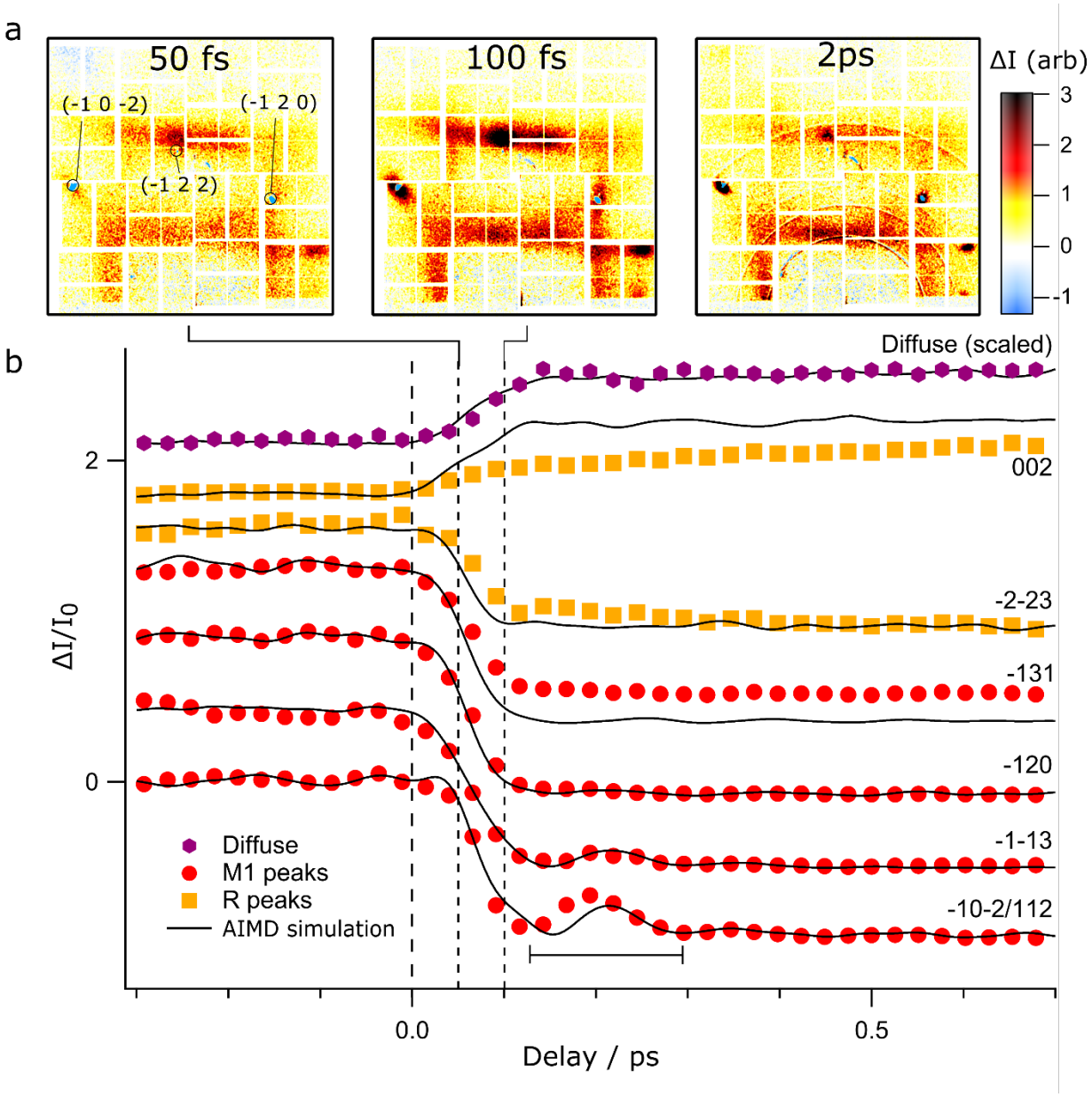

Fig. 3 Time dependence of Bragg peaks and diffuse scattering for above-threshold pumping of 22 mJ/cm^2 (A) Snapshots of the increase in the diffuse intensity $\Delta I(\mathbf{Q}, t)$ at several delays after laser excitation. **(B)** Temporal evolution of selected Bragg peaks and integrated diffuse scattering signal compared to AIMD simulations (solid lines). With the exception of the diffuse scattering signal, all data is normalized to the pre-time zero amplitude for both experiments and simulations with no further scale factor. The diffuse scattering data is compared to the variance of the vanadium positions obtained from the AIMD simulations and is thus separately normalized. The horizontal bar indicates half of the period of the relevant 3THz acoustic modes of the rutile phase (see text for details). The additional Bragg peaks that do not appear in **(A)** were obtained in a different experimental geometry, shown in Fig S3.

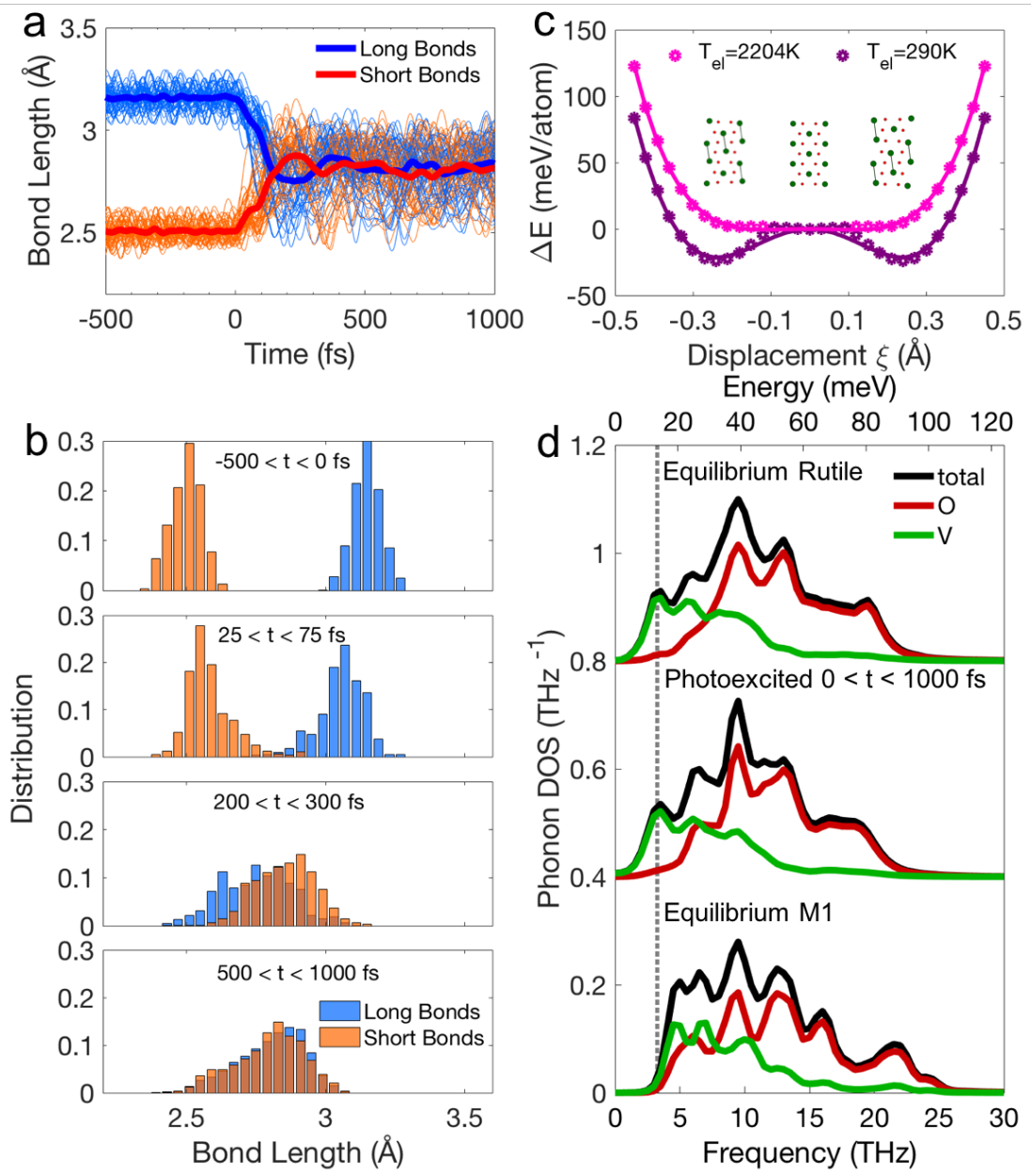

Fig. 4 Simulated VO2 response under photoexcitation, based on first-principles DFT simulations. (**A**) Time evolution of dimer bond lengths from ab-initio molecular dynamics. Short (d_S) and long (d_L) bonds are indicated in Fig 1a. (**B**) Distribution of dimer bond lengths from (**A**), integrated over several time intervals before and after photoexcitation. The merging of the distributions after a brief overshoot is evident, indicating the evolution toward the rutile phase with chains of equidistant V atoms. (**C**) Effect of photoexcitation on the potential for the distortion coordinate **ξ**. Rutile corresponds to **ξ** =0 Å and M1 to either **ξ** = +/- 0.24 Å. The photoexcitation lifts the two M1 minima of the double-well potential to stabilize the rutile phase in a flat, strongly quartic potential. Markers are DFT energies and curves are polynomial fits. (**D**)

Phonon density of states, and elemental decomposition on V and O atoms, obtained from AIMD trajectories for the equilibrium M1 phase before photoexcitation (bottom) and after photoexcitation (middle). The appearance of the pronounced V vibration peak at 3 THz (dashed line) after photoexcitation is characteristic of the rutile phase equilibrium phonon dynamics, shown in the top curves (T=380K)